remote sensing

MDPI

Article

Estimation of Water Use in Center Pivot Irrigation Using Evapotranspiration Time Series Derived by Landsat: A Study Case in a Southeastern Region of the Brazilian Savanna

Marionei Fomaca de Sousa Junior *, Leila Maria Garcia Fonseca and Hugo do Nascimento Bendini

National Institute for Space Research (INPE), São Jose dos Campos 12227-010, Brazil
* Correspondence: marionei.junior@inpe.br

Abstract: In Brazil, irrigated agriculture is responsible for 46% of withdrawals of water bodies and 67% of use concerning the total water abstracted volume, representing the most significant consumptive use in the country. Understanding how different crops use water over time is essential for planning and managing water allocation, water rights, and farming production. In this work, we propose a methodology to estimate water used in agriculture irrigated by center pivots in the municipality of Itobi, São Paulo, in the Brazilian Savanna (known as Cerrado), which has strong potential for agricultural and livestock production. The methodology proposed for the water use estimate is based on mapping crops irrigated by center pivots for the 2015/2016 crop year and actual evapotranspiration (ETa). ETa is derived from the Operational Simplified Surface Energy Balance model (SSEBop) and parameterized for edaphoclimatic conditions in Brazil (SSEBop-Br). Three meteorological data sources (INMET, GLDAS, CFSv2) were tested for estimating ETa. The water use was estimated for each meteorological data source, relating the average irrigation balance and the total area for each crop identified in the map. We evaluated the models for each crop present in the center pivots through global accuracy and f1-score metrics, and f1-score was more significant than 0.9 for all crops. The potato was the crop that consumed the most water in irrigation, followed by soy crops, beans, carrots, and onions, considering the three meteorological data sources. The total water volume consumed by center pivots in the municipality of Itobi in the 2015/2016 agricultural year for each meteorological data source was 3.2 million m^3 (INMET), 2.5 million m^3; (GLDAS), and 1.8 million m^3 (CFSv2).

Keywords: water resources; remote sensing; Landsat; SSEBop-Br model; crop water use; irrigation

check for updates

Citation: de Sousa Junior, M.F.; Fonseca, L.M.G.; Bendini, H.d.N. Estimation of Water Use in Center Pivot Irrigation Using Evapotranspiration Time Series Derived by Landsat: A Study Case in a Southeastern Region of the Brazilian Savanna. *Remote Sens.* **2022**, *14*, 5929. https://doi.org/10.3390/rs14235929

Academic Editors: Luca Brocca, Julian Koch, Christian Massari, Manuela Girotto, Jacopo Dari and Sara Modanesi

Received: 17 September 2022
Accepted: 1 November 2022
Published: 23 November 2022

Publisher's Note: MDPI stays neutral with regard to jurisdictional claims in published maps and institutional affiliations.

Copyright: © 2022 by the authors. Licensee MDPI, Basel, Switzerland. This article is an open access article distributed under the terms and conditions of the Creative Commons Attribution (CC BY) license (https://creativecommons.org/licenses/by/4.0/).

1. Introduction

According to surveys carried out by the National Agency for Water and Basic Sanitation (ANA) [1], irrigation is responsible for about 50% of water abstraction from springs in Brazil. Studies have identified an area of 76.2 million hectares with potential expansion for irrigated agriculture [1,2]. However, this whole expansion scenario must be carefully evaluated to ensure national water security through water resource management. In many producing regions, current irrigation practices are not sustainable and even under the most efficient scenarios water abstraction rates remain unsustainable [3,4]. Although Brazil has the largest sources of fresh water in the world, about 70% is distributed in the Amazon region, while the remainder is distributed to about 95% of the country's population. Due to its large territorial extension, several conflicts in water use have been observed, mainly those related to agricultural irrigation. These conflicts have been more evident in the Northeast and Southeast Regions of Brazil [5].

In this context, water use estimate in irrigated crop areas has been an essential tool for water resource management. Actual evapotranspiration (ETa) is a key variable in this process, which describes all processes in which liquid water at or near the land surface becomes atmospheric water vapor under natural conditions [6]. Estimation of and mapping

the spatiotemporal distribution of ETa over large areas has been a challenge due to the great spatial heterogeneity of variables used in the models, as well as the lack of calibration and validation data in Brazil [7]. However, remote sensing technologies allow consistent analysis at a lower cost when compared to methods based on field measurements [8]. In addition, technological advances based on cloud processing, such as the Google Earth Engine (GEE) platform, and ETa estimation based on moderate spatial resolution thermal data have allowed water use estimation to be more efficient for large areas [9,10].

Nevertheless, there are still few scientific studies based on remote sensing technologies to estimate water use in large irrigation areas. In Brazil, ANA [11] estimated the water use in irrigated agricultural areas in three accumulated periods (May to August 2018, May to September 2018, and October 2018 to January 2019) from 25 pivots located in the Brazilian Cerrado. In this context, Cassola [12] estimated the water use in agricultural areas irrigated by center pivots in the south of Brazil, using possible agricultural scenarios based on evapotranspiration data obtained from a meteorological station next to the pivot region. Schauer and Senay [9] performed the spatiotemporal dynamics characterization of water use in irrigated agricultural areas, combining annual ETa with crop classification in the Central Valley, California.

Several studies on agricultural mapping based on vegetation indices (VI) and time series derived from the Moderate Resolution Imaging Spectroradiometer (MODIS) sensor have been proposed in the literature [13–17]. However, its low spatial resolution (250–1000 m) is not appropriate for mapping small agricultural areas [18]. Bendini et al. [19] proposed a method for mapping different crops in the Cerrado region using phenological metrics extracted from dense VI time series (temporal resolution of 8 days) obtained from Landsat 7 and 8 satellite images, with an accuracy greater than 90%. Phenological metrics allowed us to infer the crop permanence time in the field as well as the beginning and end of the cycle. This approach is consistent and robust and has been used to analyze cropping patterns within the Cerrado pivots, the results of which were published in the second edition of the *Irrigation Atlas* [1].

Regarding the ETa estimate, ANA and the United States Geological Survey (USGS) adapted the Operational Simplified Surface Energy Balance model to the Brazilian morphoclimatic reality, named SSEBop-Br [11]. Among the models that use energy balance variables to obtain ETa at a large scale, the SSEBop model is one of the simplest, as it does not solve the energy balance completely [20]. SSEBop estimates ETa from the evapotranspiration (ETf) fraction obtained from Landsat thermal data and the traditional crop coefficient (Kc) and the reference evapotranspiration (ETr) estimated by the Penman–Monteith (P-M) method for an alfalfa or grass surface [21,22].

Therefore, in this study, we aim at estimating the water use in agricultural areas irrigated by center pivots in the municipality of Itobi, São Paulo, in the Cerrado region, for the 2015/2016 crop year. In agricultural areas irrigated by center pivots in the Brazilian Cerrado, up to three crop cycles can be observed in a single crop year. Hence, in this work, it is essential to determine the crop planting and harvesting dates to better estimate the water use in each cycle. Agricultural mapping methods based on phenological metrics extracted from VI time series are very adequate for mapping multiple crop cycles [19]. The water use estimation methodology implemented in our approach involves an adaptation and integration of the methods proposed by Schauer and Senay [9] and by Bendini et al. [19]. We used the method proposed by Bendini et al. [19] to obtain a crop classification map. However, we also used phenological metrics to determine the period that the crop was cultivated in the field. We propose a methodology capable of being replicated on larger scales, as we have the necessary data.

2. Study Area and Datasets

2.1. Study Area

The study area comprises the municipality of Itobi (13,844 ha) in the state of São Paulo and Cerrado biome. The region is in the Tambaú-Rio Verde, a sub-basin located in the

southeast of the Rio Pardo Basin (Figure 1). In this region, the predominant climate class is Cwa, characterized as hot subtropical and dry winter [23]. The average annual precipitation is 1517 mm, with the rainy season occurring from October to March and the rain peak in December. The dry season occurs from April to September and the lowest precipitation occurs in July and August [24].

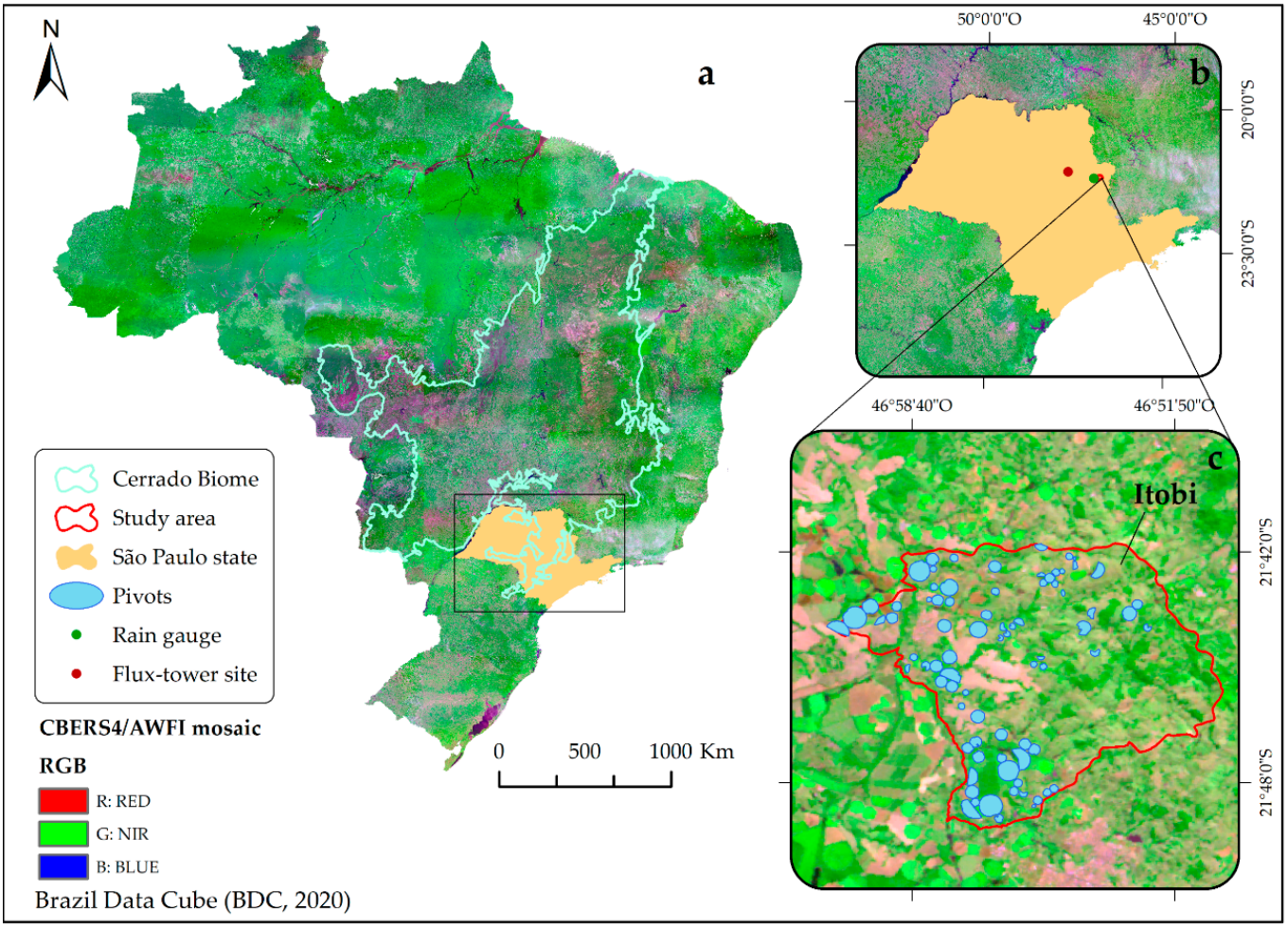

Figure 1. (**a**) Study area located in the Brazilian Savanna highlighted in the center of Brazil's map. The black rectangle indicates the state of São Paulo; (**b**) indicates the municipality of Itobi and rain gauge and flux-tower sites; (**c**) indicates the municipality of Itobi and the center pivots that were analyzed.

The study area comprises the irrigation pole of Rio Pardo and Mogi Guaçú, covering an area of 1,097,088 ha and an irrigated area of 129,287 ha. This irrigation pole has a total and effective potential of 232,575 ha and 65,989 ha, respectively, and is considered one of the poles with the greatest expansion perspective [1,2]. Center pivot irrigation is predominantly used for vegetable cultivation, mainly potatoes and onions, from March to October. In the last two decades, the number of center pivots and total irrigated increased in this region. However, this region is prone to water use conflicts because the Tambaú-Rio Verde sub-basin has high water demand, i.e., consumption is greater than 50% of Q7,10 (the lowest average streamflow during 7 days with an average recurrence of 10 years) [25]. In addition, the hub extrapolates the federation unit and contains water bodies under the Union's domain, requiring even more integrated efforts in water resource management and planning.

2.2. Datasets

Enhanced Vegetation Index (EVI) images [26] were obtained from the GEE platform, through the QGIS plugin, GEE Time Series Explorer (https://geetimeseriesexplorer.readthedocs.io, accessed on 15 October 2021), for Landsat 7 and 8 satellites [27]. Images acquired in the 2015/2016 agricultural year from August 2015 to October 2016 were selected, considering the availability of field data to train the crop classification model. ETa images were obtained from SSEBop-Br v.1.01 application, which is integrated into the GEE platform (https://ssebop.users.earthengine.app/view/ssebop-br-v101, accessed on 10 May 2021). The center pivot irrigated agriculture mask was obtained from the center pivots irrigated agriculture map, for the year 2014, available on the ANA's site (https://dadosabertos.ana.gov.br, accessed on 15 October 2021). In this work, we supposed that the mask did not change for the agricultural year 2015/2016.

To evaluate the SSEBop-Br model, we employed ETa data measured in a flux-tower site (Figure 1) located in a sugarcane area belonging to the Santa Rita Electric Company (21.63°S, 47.78°W, altitude of 552 m). Around the flux tower, the sugarcane plantation is homogeneous in all directions within a radius of 500 m. The average canopy varies by 3.5 m, from crop emergence to harvest [24,28]. The major components of the conservation of energy equation, often referred to as 'energy-balance closure', are radiation balance (Rn), ground heat flux (G), convective sensible heat exchange (H), and latent heat exchange or evapotranspiration (LE) [29]:

$$Rn = H + LE + G + S \quad (1)$$

where S is the heat storage in the canopy. The variables are measured every 30 min in the flux tower.

To obtain the ETa, the surface energy balance was closed and then H and LE were calculated through the Bowen ratio method (β = H/LE), as described in [29]. Cases in which more than 5 observations were missing during the day (8:00–18:00 h), the entire day was disregarded in the analysis [30,31]. The surface energy balance close to eddy covariance systems often presents errors, probably due to the data collection time, location and land cover characteristics, measurement uncertainties, and soil heat storage [29,31,32]. After correcting the energy balance variables, ETa and Kc were obtained from the fraction of observed ETr and the eddy covariance system, respectively. ETa data were integrated at a daily scale.

To calculate the irrigation balance, we used rainfall data from INMET's A738 meteorological station, located in the municipality of Casa Branca, SP (21.78°S, 47.08°W, altitude of 734 m) (Figure 1). The A738 station in the municipality of Casa Branca was chosen due to the lack of in situ stations in the study area. In addition, we used field data acquired during the 2015/16 harvest in the city of Itobi, SP, to train the crop classification model. In the study area, agricultural dynamics were analyzed in three visits during the year. In each visit, the sample coordinates were collected with a GNSS device, and crop rotation information in the center pivots was provided directly by producers. Field boundaries were identified in the satellite images through visual interpretation. The fieldwork protocol area is available in Sanches et al. [33]. All 33 polygons were identified to represent the 7 types of crops grown in the period 2015/2016 in the pivots. About 50 random pixels with a minimum distance of 30 m within each polygon were selected, as shown in Table 1. As described in [18], a negative buffer of 30 m was applied to them to avoid spectral mixing in the polygon edges.

Considering the pivot mask, a hexagonal sampling was performed to represent the entire pivot area, which resulted in an average of 16 points per center pivot. A total of 1294 points in 80 pivots located within the study area were selected. As this approach analyzes a set of points in each center pivot area, the processing steps require less computational effort. The area of a given pivot is linearly proportional to the number of points

sampled evenly within the pivot. Points were obtained within a buffer 30 m away from the pivot edges. Afterward, EVI time series data were extracted for each sample point.

Table 1. Definition of the crop rotation (classes), crop type, and the number of samples for training and validation of the model.

Crop Rotation	Samples	Crop Type
Maize + Beans	143	First crop + Winter crop
Maize + Carrot	86	First crop + Winter crop
Maize + Onion	91	First crop + Winter crop
Maize + Potato	183	First crop + Winter crop
Soy + Potato	612	First crop + Winter crop
Maize + Soy	284	First crop + Second crop
Soy	81	Single crop

3. Methods

Considering both irrigation water use and agricultural mapping processes, Figure 2 shows all steps of the methodology proposed in this work.

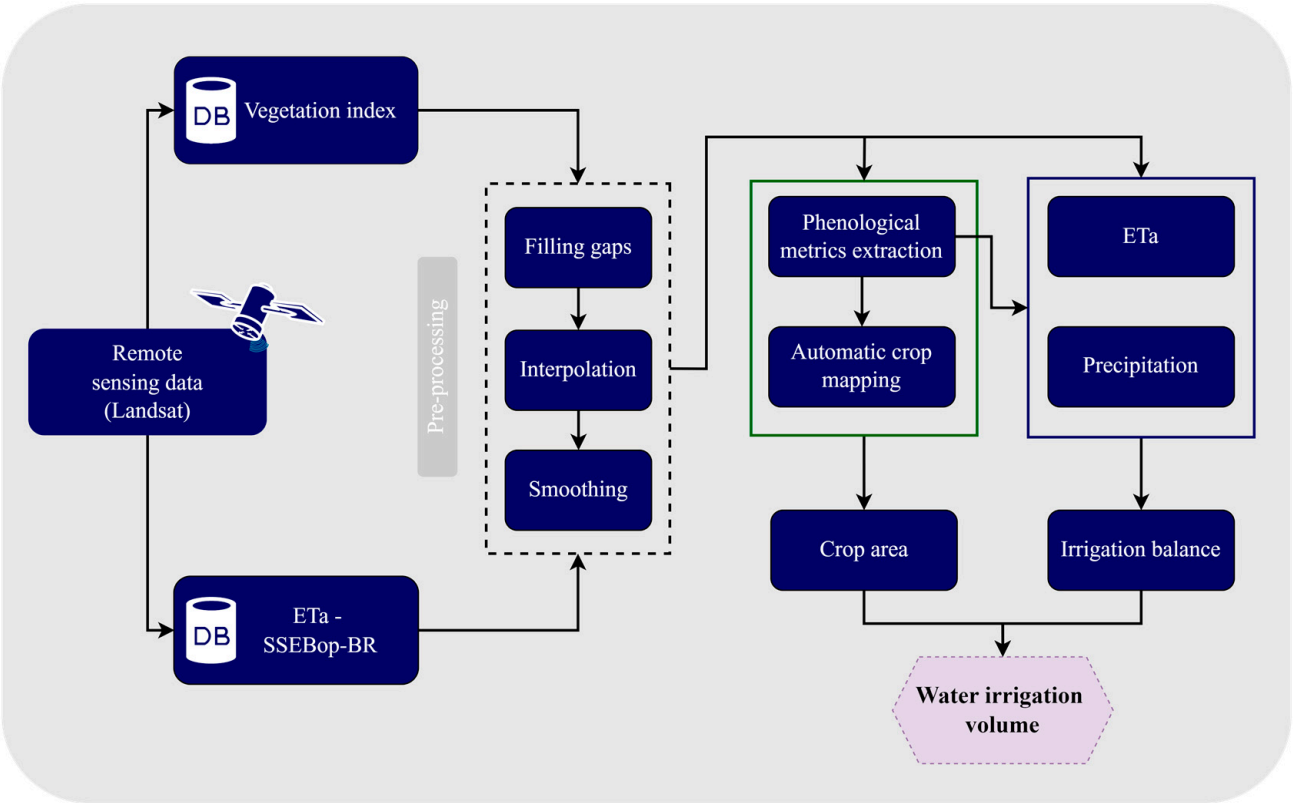

Figure 2. General scheme of the methodology used to estimate water use in irrigation. The dashed rectangle indicates the pre-processing steps of the time series (ETa and EVI). The green rectangle indicates the processes for obtaining the crop area. The blue rectangle indicates the process of ETa and precipitation accumulation according to cycle duration based on phenological metrics.

3.1. Crop Classification and Phenological Metrics

The crops present in each center pivot analyzed in this work are classified based on the methodology proposed by [19]. The authors used a hierarchical classification based on Random Forest with four levels, from land cover to crop rotation classes. Most of the classes showed accuracies higher than 90%. They showed that phenometrics derived from dense

Landsat-like image time series, in a hierarchical classification scheme, have great potential for detailed agricultural mapping. The flowchart of the processing steps for mapping crops in the center pivots is shown in Figure 3.

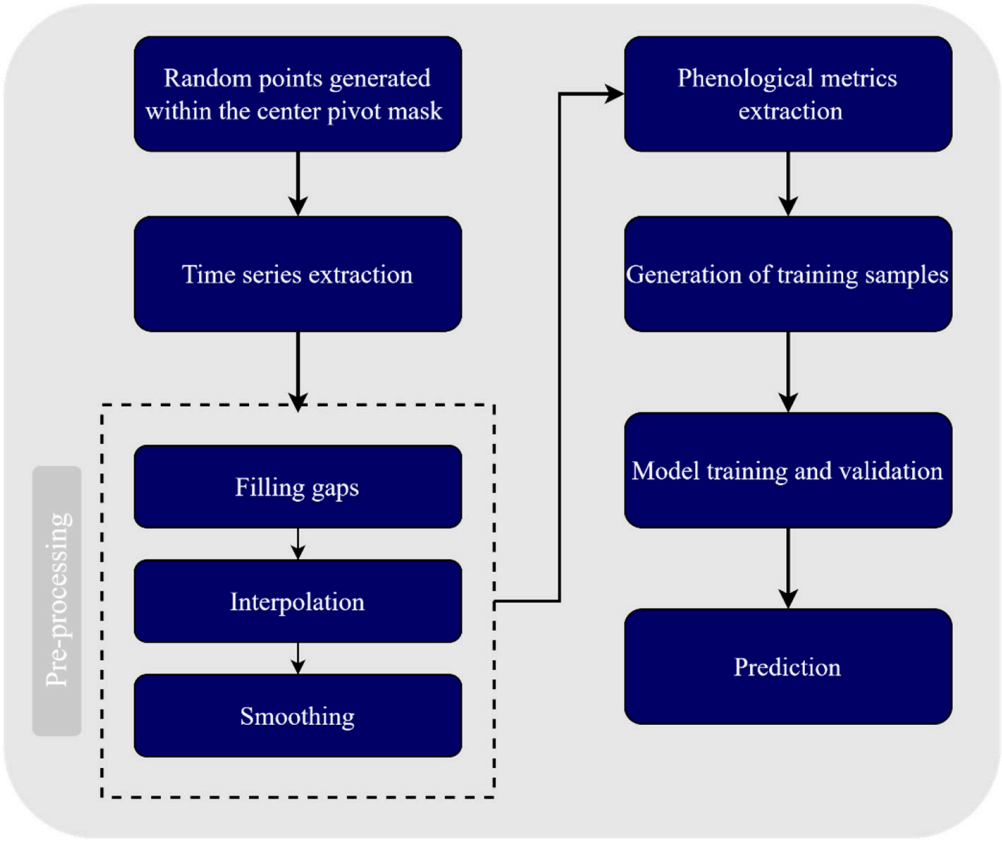

Figure 3. Flowchart of processing steps for mapping crops in the center pivots.

Phenological metrics were extracted from the EVI time series using the Stmetrics package (https://github.com/brazil-data-cube/stmetrics, accessed on 20 October 2021), implemented in Python language [34]. Thirteen phenological metrics were extracted for each cycle in the analyzed period. Table S1 presents a summary of the metrics used in the agricultural mapping process [35,36].

The classification algorithm requires time series with regular time intervals and without noise. To reduce noise in the EVI time series caused by clouds, cloud shadows, and Scan Line Corrector (SLC) failure in Landsat 7, the Kalman filter was used [37]. Subsequently, bicubic spline interpolation [38] was applied to obtain time series with observations regularly spaced in time, at a regular interval of 8 days for the period of analysis, totaling 57 observations. Finally, the time series data were smoothed with the Savitzky–Golay filter [35], with a window size equal to 4. For the study area, pivots with one or two harvests were observed in the 2015/2016 crop year. The double crop was represented by the 1st cycle in the summer with the 2nd cycle soon after, or the 1st cycle in the summer with the 2nd cycle in the winter.

After extracting the phenological metrics, the Random Forest (RF) model [39] was trained using field samples collected in the center pivots. The classification was performed in R programming language using the Random Forest package [40], with parameters ntree and mtry equal to 90 and 5, respectively [19]. The parameter ntree represents the number of decision trees to be generated, which is determined by observing error stabilization. The mtry parameter represents the number of variables to be selected and tested for the best split during the growth of the trees [41]. The model evaluation was performed using metrics based on the confusion matrix after applying Monte Carlo simulation [42]. In this

case, the model was trained 1000 times, randomly selecting 70% of the data for training and 30% for validation. In each simulation, the global accuracy of the model [43] and the f1-score [44] for each class were calculated. Afterward, the mean global accuracy values and f1-score were calculated.

For each class, its area was obtained proportionally to the number of points classified within each pivot, as shown in Figure 4. For example, if 100% of points within a pivot are classified as a given class, the area for this class in that pivot is equal to the total area of the pivot.

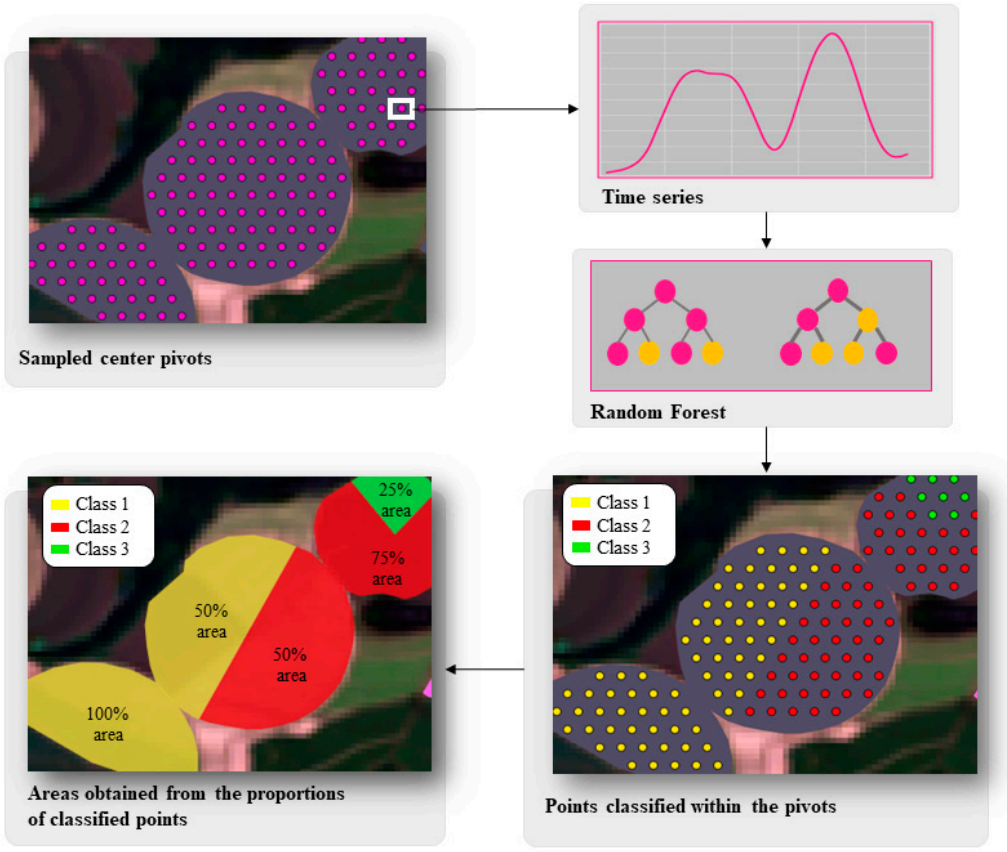

Figure 4. Flowchart of agricultural mapping in each center pivot.

3.2. ETa Estimation and SSEBop-Br Assessment

ETa images were obtained through the SSEBop-Br model, which is integrated into the GEE platform. According to [22], the SSEBop-Br model estimates ETa as follows:

$$ETa = ETf \times ETr \quad (2)$$

Equation (2) combines Landsat thermal data used in ETf estimation (range from 0 to 1) and climatic data used in the ETr estimation by P-M method for an alfalfa or grass surface. The P-M method uses climatological data, e.g., solar radiation, air temperature, humidity, and wind speed. In SSEBop-Br, we used ETr based on grass surface compiled by Xavier et al. [45]. The SSEBop-Br model stands out for solving the latent heat flux without the need to solve the other components of the energy balance. This model redefines the limits of the difference between hot and cold reference pixels for each pixel, unlike traditional models based on energy balance, which establish a set of hot and cold pixels for a limited region [46].

The climatic data used in the ETr calculation are derived from 3 data sources: a grid built from meteorological stations of the National Institute of Meteorology (INMET), the Global Land Data Assimilation System (GLDAS), and the National Centers for Environ-

mental Prediction Climate Forecast System (CFSv2). To analyze the differences between the model results obtained by different data sources, the ETa estimate was calculated for each one of them.

Processing ETa time series is similar to processing EVI time series, except for the bi-cubic spline function [38], which is used to generate time series with daily observations to obtain the ETa accumulated throughout the crop cycle. ETa values estimated by the SSEBop-Br model were compared to ETa values obtained by a flux tower located in a sugarcane area (Figure 1). Model evaluation was performed based on the mean absolute error (MAE) [47], bias [48], Willmott agreement index [49], and Nash–Sutcliffe coefficient (NSE) [50].

MAE measures the error magnitude of the estimate, in the same unit as the analyzed variable:

$$MAE = \frac{1}{n} \sum_{i=1}^{n} |S_i - O_i| \quad (3)$$

where MAE is the mean absolute error (mm); S_i is the ETa value estimated by the model (mm); O_i is the ETa value observed in the field (mm). The closer to zero, the better the fit concerning the observed series.

PBIAS measure indicates whether there is an under- or overestimation of the reference data in percentage:

$$PBIAS = 100 \sum_{i=1}^{n} \frac{|S_i - O_i|}{O_i} \quad (4)$$

The Willmott (dimensionless) agreement index, d, is a normalized measure of the degree of prediction error in a model:

$$d = 1 - \frac{\sum_{i=1}^{n} (O_i - S_i)^2}{\sum_{i=1}^{n} (|S_i - O| + |O_i - O|)^2} \quad (5)$$

where O is the mean of the ETa values observed in the field. Values of "d" equal to 1 indicate a perfect fit to the observed data [48].

The normalized index, NSE, determines the relative magnitude of the residual variance compared to the variance in the observed data [49]:

$$NSE = 1 - \frac{\sum_{i=1}^{n} (O_i - P_i)^2}{\sum_{i=1}^{n} (O_i - O)^2} \quad (6)$$

where NSE is the Nash–Sutcliffe (dimensionless) coefficient.

To evaluate data concerning NSE values, Van Liew et al. [51] propose the following classification: NSE = 1 means perfect fit of the data predicted by the model; NSE > 0.75 indicates that the model is adequate and good; 0.36 < NSE $\leq$ 0.75 indicates that the model is considered satisfactory; and NSE < 0.36 indicates that the model is not satisfactory.

3.3. Irrigation Balance and Water Use

The irrigation balance represents the difference between the ETa and the accumulated precipitation. The start and end dates of the cycle used in the aggregation of ETa and precipitation were obtained through the metrics Strt and End. The Strt metric represents the moment when a significant increase in the rise of the EVI curve is observed, and not the actual planting date. On the planting date, there is not enough plant response to be expressed by the vegetation index. Thus, the actual planting date was empirically estimated by subtracting 15 days from the date corresponding to the Strt metric [52]. Therefore, irrigation balance is calculated assuming that all precipitation that occurred in the cycle was effective, knowing that this may underestimate water use [9]. In addition, we considered the return flow is negligible in the sprinkler-irrigated field [53], which is the type of irrigation present in center pivots in our study area.

The irrigation water estimate was based on the methodology proposed by [9], in which the authors relate the ETa obtained by the SSEBop model with crop area, as follows:

$$Water\ volume = \frac{Irrigation\ balance\ \times\ Crop\ area\ \times\ 10}{0.85} \quad (7)$$

where Water volume is water used to irrigate a crop in a given cycle (m^3), and irrigation balance is the difference between the average accumulated ETa for points classified as a given crop (mm) and accumulated precipitation (mm). Crop area is the estimated area of a given crop (ha), 10 is the conversion factor, and 0.85 is the adopted efficiency of a center pivot [11].

4. Results

4.1. SSEBop-Br Assessment

Table 2 shows performance measures of the SSEBop-Br model to produce ETa in the sugarcane crop under a rainfed regime. Figure 5 presents a comparison between estimated and observed data, considering three data sources, named INMET, GLDAS, and CSFv2. Figure 6 shows the evapotranspiration profile observed in the field and estimated by SSEBop-Br.

Table 2. Validation of ETa based on SSEBop-Br model for the three sources of meteorological data available.

Data Source	MAE	RMSE	NSE	PBIAS	r^2
GLDAS	0.40	0.49	0.88	−12.10	0.95
INMET	0.53	0.66	0.77	20.20	0.98
CFSv2	0.59	0.91	0.57	15.70	0.94

MAE e RMSE em mm d^{-1}.

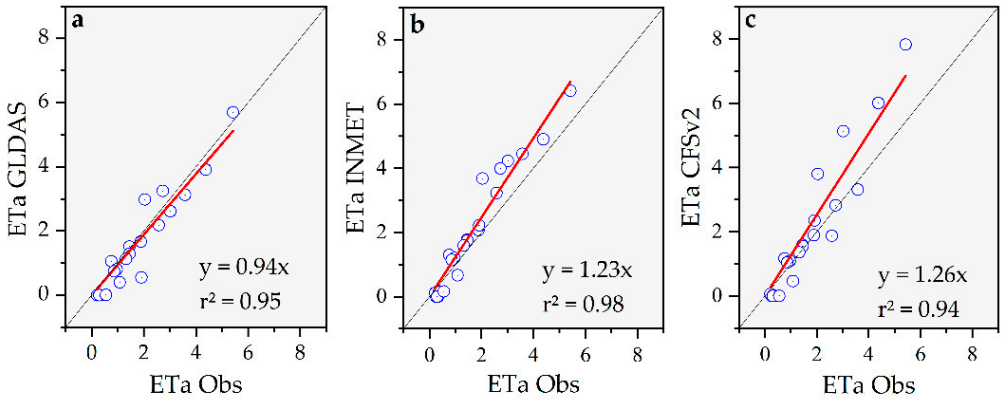

Figure 5. Comparing ETa estimated by the SSEBop-Br model for the three sources of meteorological data, (**a**) GLDAS, (**b**) INMET, (**c**) CSFv2, and ETa observed in a flux-tower site.

The estimated ETa using INMET data explained 98% of the values observed in the field, followed by GLDAS data (95%) and CFSV2 (94%). When observing the trend line concerning the 1:1 straight line, one can observe that ETa estimation based on INMET and CSFV2 data tends to overestimate ETa. For GLDAS data, one can observe the best fit of the trend line, indicating greater proximity between the data observed in the field and the data estimated by the SSEBop-Br model. The CFSv2 model showed greater overestimation during the crop growth phase, which occurred during the rainy season, with the highest ETa values. The INMET model presented a tendency to overestimate the ETa values during most of the cycle. PBIAS values corroborate these results, in which ETa values based on INMET and CFSv2 data were overestimated at 20.2% and 15.7%, respectively, while GLDAS data underestimated ETa values at 12.1%. Although ETa values based on INMET data

showed higher r^2, one can observe in Table 2 that ETa values based on GLDAS data resulted in lower MAE and RMSE values, as well as the highest NSE coefficient.

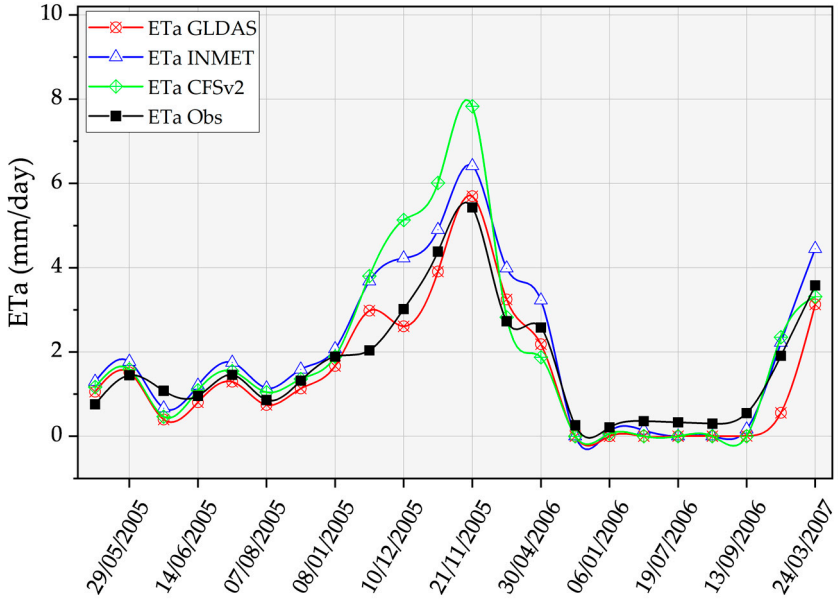

Figure 6. ETa profile estimated by SSEBop-Br model for the three sources of meteorological data (GLDAS, INMET, and CSFv2) and ETa observed in a flux-tower site.

Oliveira [31] estimated ETa for this same study area and under the same conditions as the present work using the METRIC model in two scenarios: (1) using meteorological data as input to the model, obtained from the micrometeorological tower itself, and (2) using GLDAS meteorological data. In the first scenario, r^2 equal to 0.95, MAE equal to 0.21 mm d^{-1}, and RMSE equal to 0.35 mm d^{-1} were obtained, when compared to ETa estimated by the METRIC model and field data. In the second scenario, Eta values were overestimated in 25%, and obtained r^2, MAE, and RMSE values equal to 0.86, 1.03 mm d^{-1}, and 1.17 mm d^{-1}, respectively. Table 2 shows an opposite behavior (underestimation) when GLDAS data were used as input to the SSEBop-Br model. Oliveira [31] states that the overestimation results for the METRIC model are due to the automatic selection of cold pixels for the internal calibration of sensible heat (H).

4.2. Crop Mapping and Area Estimates

The total area and the average area of pivots in the study area are 1584.3 and 20 ha, respectively. The average area of pivots in the Cerrado biome is 68.8 ha, 70.1% greater than the average area of pivots in the study area. The profile illustrated in Figure 7 shows the cropping pattern in the summer crop season and the second season soon, represented by the class maize + soy. The maize planting was conducted from September to November, while the harvest took place mostly in January and February. Soy planting occurred soon after the maize harvest, in June and July. For the cropping pattern characterized by the first cycle of summer and second cycle of winter, the first cycle planting, represented mainly by maize, took place between September and December, while the harvest took place between February and April. In this work, winter cycles are represented by potato, onion, carrot, and bean crops, the planting periods of which vary mainly between May and July and the harvesting of which occurs in September and October. These cultivation periods corroborate Silveira et al. [54], who carried out the center pivot identification in the Tambaú-Verde watershed using remote sensing technologies. Bendini et al. [19] also obtained similar results in the analysis of the same classes, in the same place and period of the present study.

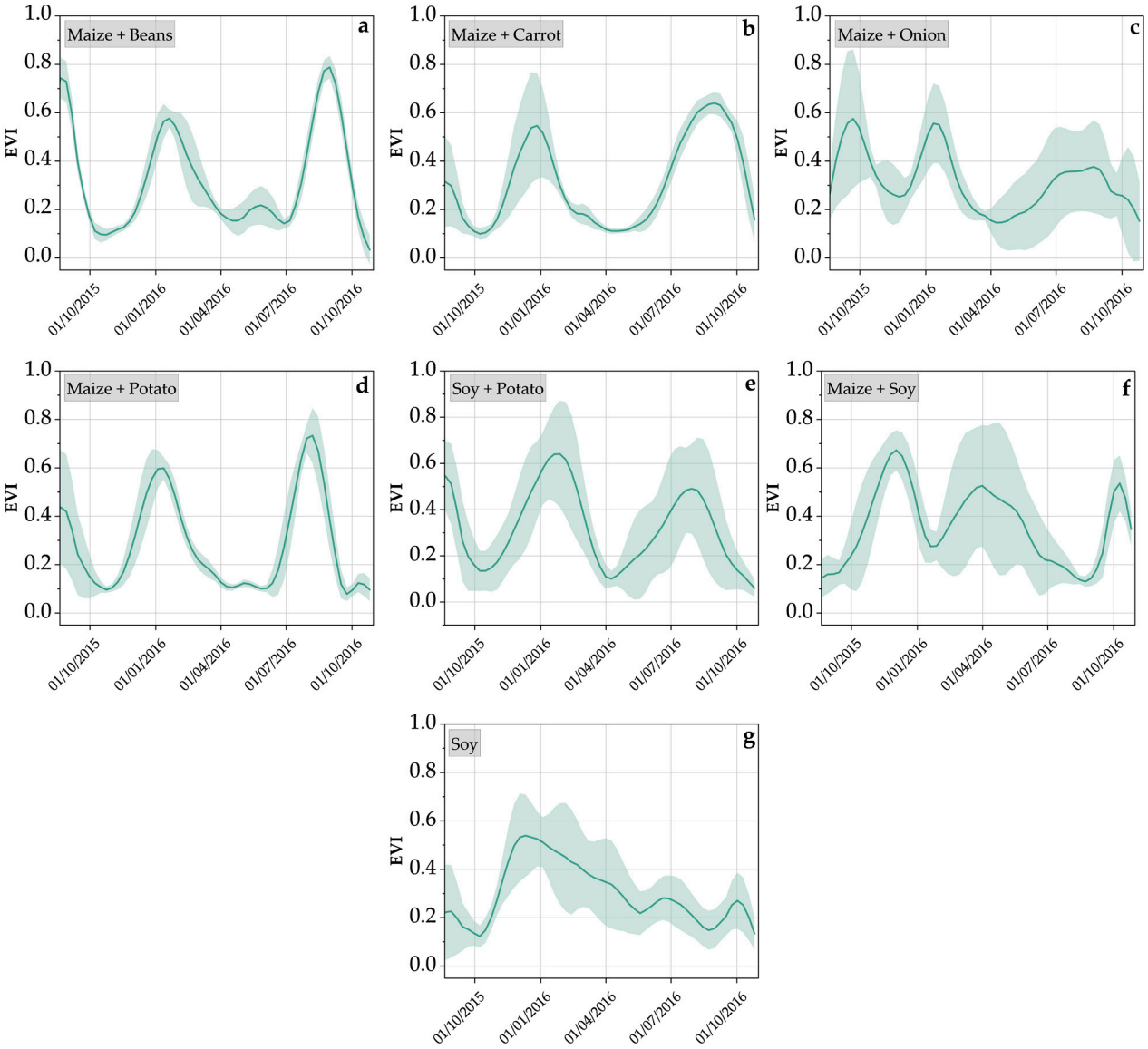

Figure 7. Mean EVI profile with its respective standard deviation for each class in the 2015/2016 agricultural year based on samples collected in the field: (**a**–**e**) represent the first crop + winter crop type, (**f**) represents the first crop + second crop class, and (**g**) shows the single crop type.

Table 3 presents the f1-score value for each class, as well as the global accuracy of the model. The results are similar to those obtained by Bendini et al. [19]. Figure 8 shows classification results in the center pivots in the municipality of Itobi, SP, for the 2015/2016 agricultural year. Figure 9 shows the total area for each class.

4.3. Water Use

4.3.1. Summer Crop Season

Figure 10 shows ETa values, rainfall, and the irrigation balance of the first cycle (soy and maize) for each meteorological data source used in the SSEBop-Br model. Regarding evapotranspiration, one can observe the highest ETa values based on the INMET data source. The lowest ETa values were obtained for the CFSv2 data source.

As observed in Figure 10, the average accumulated ETa value for the maize class (first cycle of the double crop) was 542.5 mm for CFSv2 data, 589.2 mm for GLDAS, and 634.5 mm for INMET. Radin et al. [55] obtained ETa values between 575 and 732 mm per cycle (average of 656 mm) when evaluating ETa values during four seasons. According to the authors,

the variation was mainly due to the evaporative demand in the atmosphere, which is mainly determined by solar radiation. The cycle period varied from 136 to 168 days. The maize irrigation balance was negative for all classes except for the maize + soy class, which presented balances of 4.1 and 19.9 mm based on GLDAS and INMET data, respectively.

Table 3. Global accuracy and f1-scores obtained in each class.

Class	f1-Score
Maize + Beans	0.9964
Maize + Carrot	0.9954
Maize + Onion	0.9983
Maize + Potato	0.9952
Maize + Soy	0.9998
Soy	0.9742
Soy + Potato	0.9947
Global Accuracy	0.9951

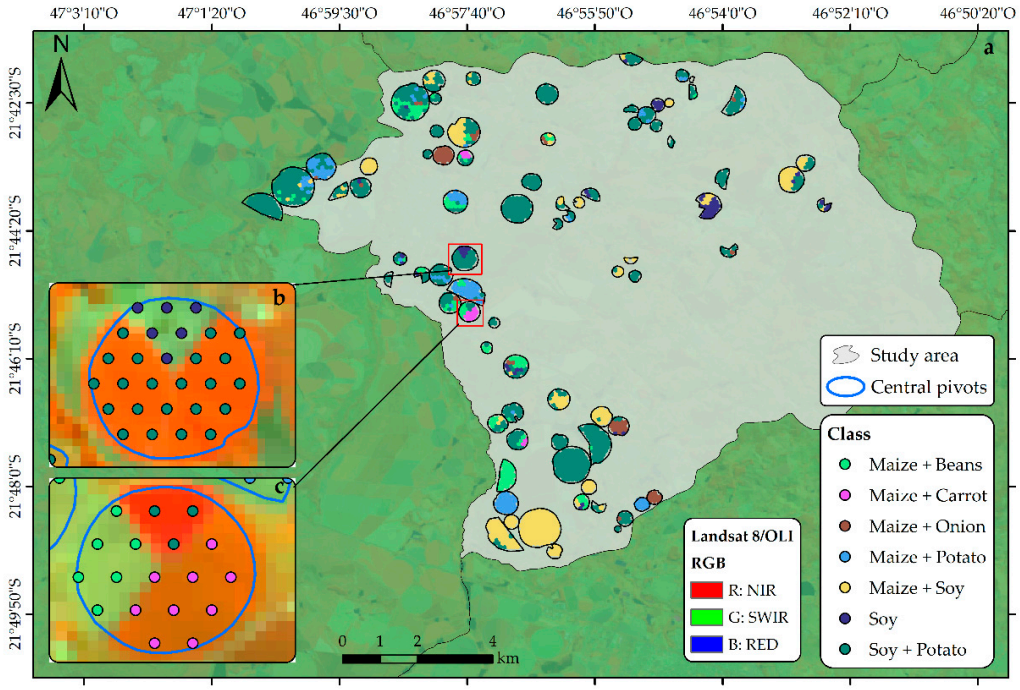

Figure 8. (**a**) Classification result in the municipality of Itobi, SP, for the 2015/2016 agricultural year. Details of the crop variability within center pivots are illustrated in figure (**b**,**c**).

In the case of soy, the average accumulated ETa values were 490 mm (CFSv2), 534.6 mm (GLDAS), and 566.52 mm (INMET). Alves et al. [56] obtained similar results when estimating ETa for soy in the Cerrado biome using the FAO 56 Dual method [57]: a value equal to 515 mm accumulated during the crop cycle. The soy cycle period varied from 131 to 137 days. The soy cycle period can vary from 70 to 180 days according to the maturation group, usually called early, semi-early, medium, semi-late, and late [58]. However, the number of days of a certain group can still vary depending on the management conditions and the soil and climate conditions of the planting region [59]. For the irrigation balance, one can observe in Figure 10 that soy, a single cycle in the agricultural year, presented positive values for GLDAS and INMET data. On the other hand, soy cultivated in a double system obtained negative values for the irrigation balance concerning all data sources.

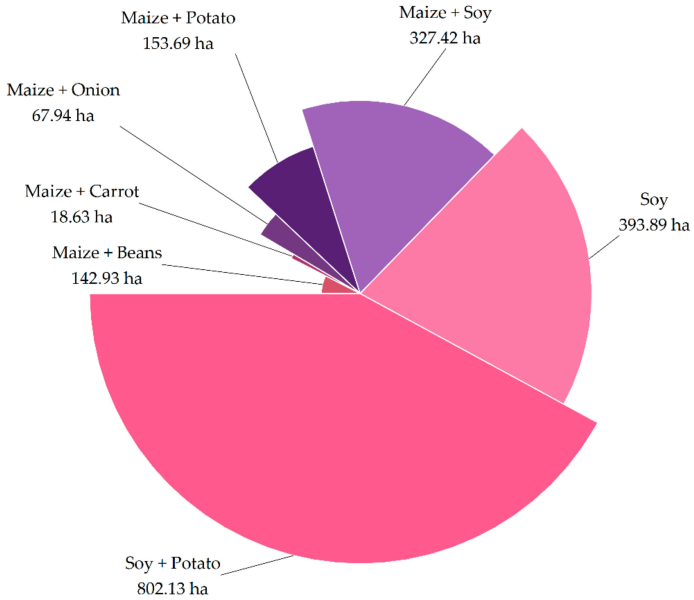

Figure 9. Crop area for each class in the 2015/2016 agricultural year.

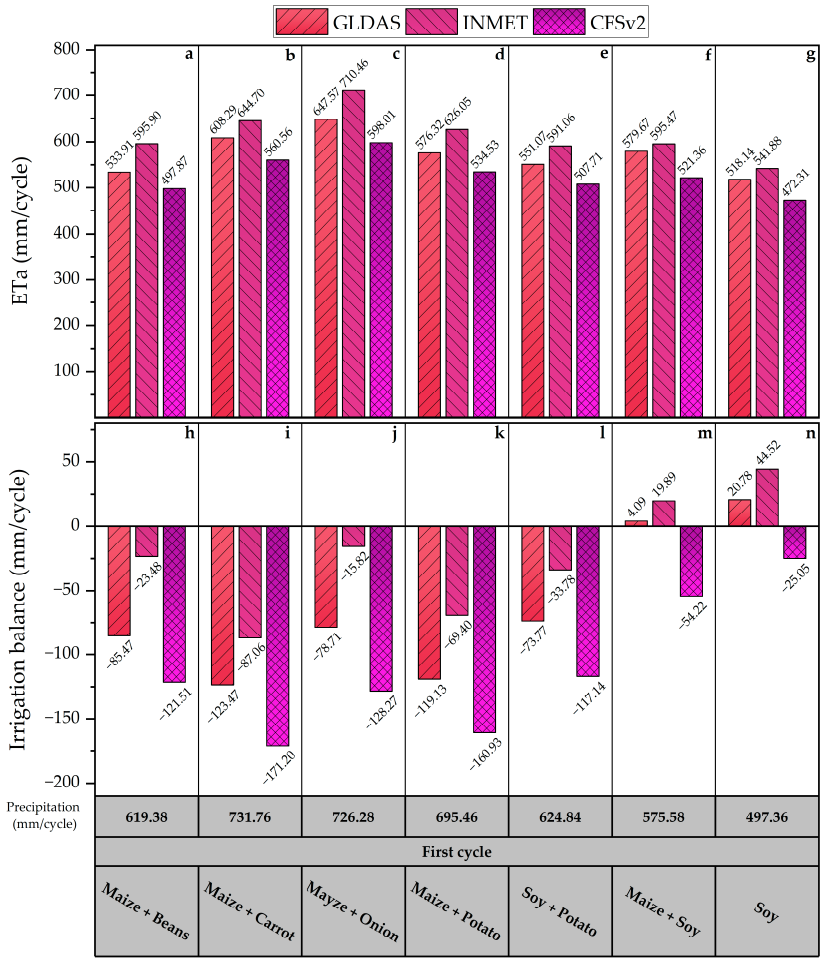

Figure 10. Average accumulated evapotranspiration (**a**–**g**), precipitation, and the irrigation balance (**h**–**n**) of the first cycle of the classes (**a**–**n**). The first cycle of the classes is mainly represented by the maize crop. The soy crop in the first cycle is observed in two classes, soy + potato and soy. The accumulated precipitation values are represented in the first row of the table below the graphs.

4.3.2. Second/Winter Season

Figure 11 shows ETa, rainfall, and the irrigation balance for the second cycle, which corresponds to winter crops (beans, carrots, onions, and potatoes) and second cycle soy (grown after maize) for each data source. Among the meteorological data sources, the INMET data obtained the highest ETa values, followed by GLDAS and CFSv2 for all crops, similarly to what occurred in the analysis of the first cycle.

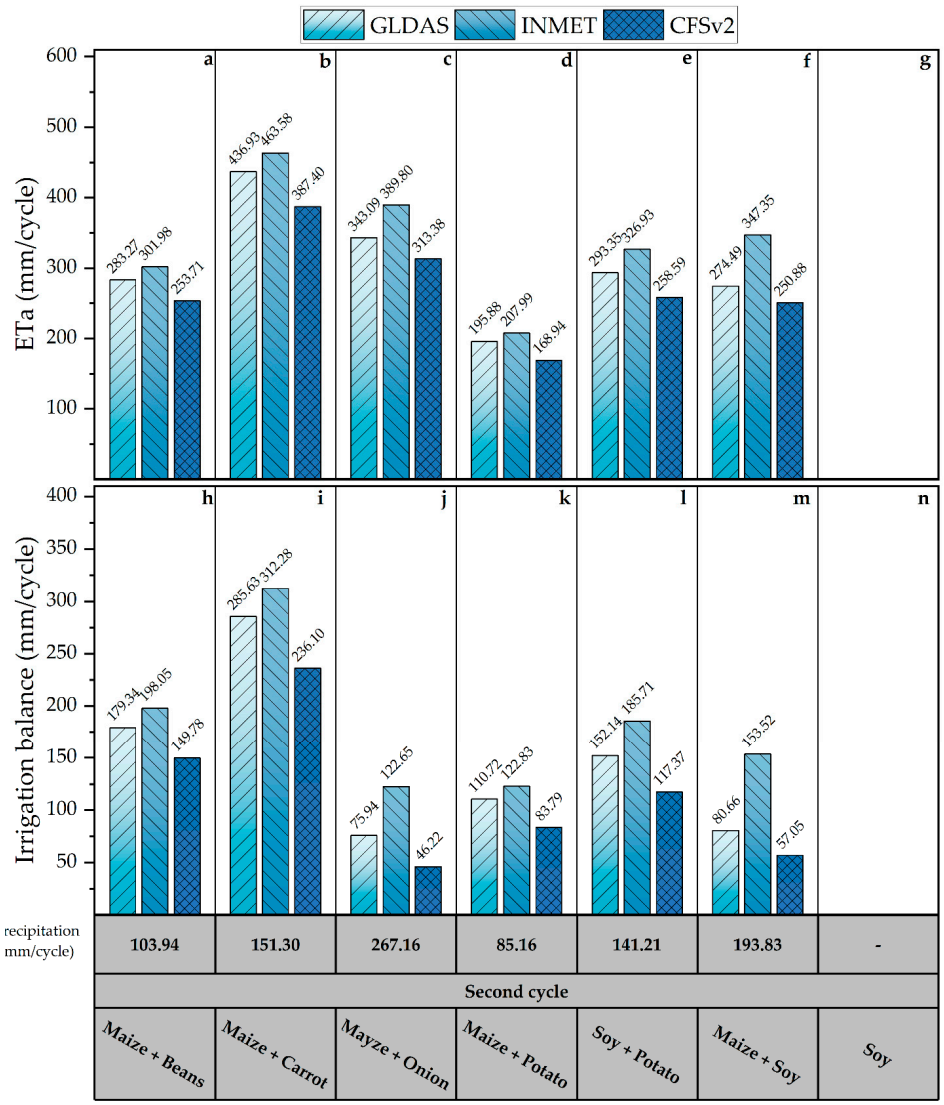

Figure 11. Average accumulated evapotranspiration (**a**–**g**) and precipitation and irrigation balance (**h**–**n**) of the second cycle of the classes (**a**–**n**). The second cycle of the classes is mainly represented by winter crops, such as beans, carrot, onion, and potato. The soy crop in the second cycle is observed in one class (maize + soy). The accumulated precipitation values are represented in the first row of the table below the graphics.

The carrot was the crop that presented the highest ETa values equal to 463.6 mm (INMET), 436.9 mm (GLDAS), and 387.4 mm (CFSv2) for a cycle of 136 days. Using a lysimeter, Lunardi and Filho [60] obtained an ETa value equal to 423 mm for the carrot cultivated in a region close to our study area, in a cycle of 117 days. On the other hand, Moura et al. [61] obtained an ETa value equal to 365 mm for a 110-day cycle.

ETa values in the carrot cycle agree with values reported by EMBRAPA [62], which reported that the crop's water requirement varies from 350 to 550 mm per cycle, depending on climatic conditions and the cycle period. Furthermore, it is highlighted that carrot is

highly sensitive to water deficit and requires soil moisture close to field capacity with water application corresponding to the evapotranspiration of the crop.

In the common bean crop, the ETa values were 302 mm (INMET), 283.3 mm (GLDAS), and 253.7 mm (CFSv2). Using drainage evapotranspirometers, Matzenauer et al. [63] obtained ETa values from 228.2 mm to 361.4 mm for the bean cycle. ETa values based on the SSEBop-Br model also agreed with values presented in [64], which varied from 250 mm to 350 mm during the cycle. The crop is highly sensitive to water stress during flowering and the beginning of pod formation and, to a lesser extent, in the vegetative phase.

The average onion crop cycle was 112 days. ETa values were equal to 389.2 (INMET), 343.1 mm (GLDAS), and 313.4 (CFSv2), which can vary according to the crop water requirement. In [65], ETa values varied from 350 mm to 650 mm and the cycle period varied from 100 to 210 days. In addition, the longest duration for late planting occurred in southern Brazil.

According to the Brazilian Potato Association (ABBA) [66], the total potato evapotranspiration varies between 250 mm and 550 mm, depending on the crop cycle length and the evaporative demand. According to ABBA [66], the cycle varies between 85 and 120 days and can be less than 85 days in seed potato production. For potato crops, the average ETa values estimated by the SSEBop-Br model were 267.5 mm, 244.7 mm, and 213.8 for INMET, GLDAS, and CFSv2 data, respectively. The potato crop cycle determined from phenological metrics varied from 80 to 112 days. Potato is considered a water-demanding crop and requires an adequate water supply during all stages of its growth.

The irrigation balance was positive for all crops in the second cycle, indicating that there was water supplementation. In terms of average consumption, the carrot was the crop that presented the highest consumption per area (mm or L/m^2;), ranging from 312.3 mm to 236.1 mm for INMET and CFSv2 data sources, respectively. Beans were the second crop that most used water per area, ranging from 198 mm (INMET) to 149.8 mm (CFSv2). The potato crop, present in two classes, used 185.7 mm (INMET) and 117.4 mm (CFSv2) in the soy + potato class, and 122.8 mm (INMET) and 83.8 mm (CFSv2) in the corn + potato class. Then, soy, cultivated after corn, presented an average irrigation balance of 153.5 mm (INMET) and 57.1 mm (CFSv2). The crop with the lowest average consumption per area was onion, varying from 122.6 mm to 46.2 mm for INMET and CFSv2 data, respectively.

4.3.3. Total Water Volume Used in the Center Pivots

Figure 12 shows the water use in the crops that showed a positive irrigation balance in the 2015/2016 agricultural year. The water use volume can be understood as irrigation balance in m^3. One can observe that there was water use in all second cycles of the agricultural year due to the lack of sufficient rainfall during the crop development period.

The potato was the crop that used the most water in the irrigation process. The water use volume was around 2 million m^3 (INMET) and 1.3 million m^3 (CFSv2). Although potato did not present the highest water use per area, it was the crop that presented the largest planted area (Figure 9). The second crop that most used water was soybean, with values ranging from 220 thousand m^3 (CFSv2) to 800 thousand m^3 (INMET). The soybean crop also had the greatest variation between the source that presented the lowest volume and the source that presented the highest estimated water volume (~264%). Therefore, the largest variations were obtained by onion (~165%) and potato (~57%) crops. This result highlights the importance of carrying out studies to assess the influence of meteorological variables used in the model to estimate water use in agricultural areas.

The water volume used in the bean crop varied from 252 thousand m^3 (CFSv2) to 333 thousand m^3 (INMET). Although the carrot crop presented the highest water use per area in irrigation (Figure 11), the total water volume was 52 thousand m^3 (CFSv2) and 68 thousand m^3 (INMET) due to the proportion of planted area in Itobi. Finally, the water use in the onion crop was 37 thousand m^3 (CFSv2) and 98 thousand m^3 (INMET).

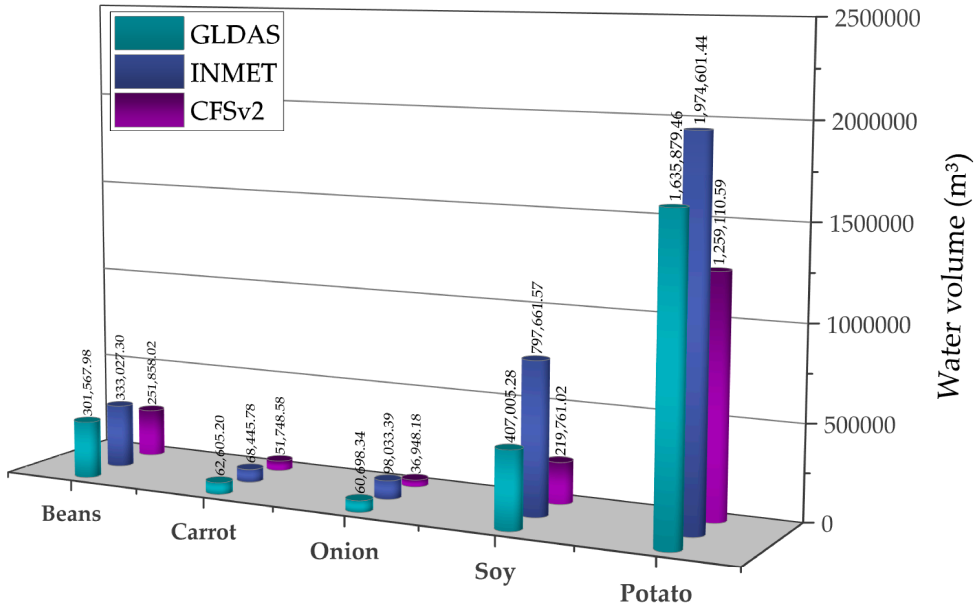

Figure 12. Water use volume estimated in the irrigation crops cultivated in the center pivots located in the study area for the agricultural year 2015/2016. The volume was estimated for crops that presented positive irrigation balance.

Finally, the total volume of water used by center pivots in the municipality of Itobi, SP, during the 2015/2016 agricultural year was equal to 3.2 million m^3 (INMET), 2.5 million m^3 (GLDAS), and 1.8 million m^3 (CFSv2), which represents a variation of approximately 78% between estimates obtained from CFSv2 and INMET data. Figure 13 shows the number of pivots and the areas irrigated by center pivots in our study area from 2000 to 2019, obtained in the Survey of Agriculture Irrigated by Center Pivots carried out by ANA [67]. From 2000 to 2019, the area irrigated by center pivots in Itobi increased by about 245%, and the number of pivots increased by about 718%. The pivot mapping used in our study was performed in 2014. From 2014 to 2019, the planted area and the number of pivots increased by approximately 9% and 13%, respectively.

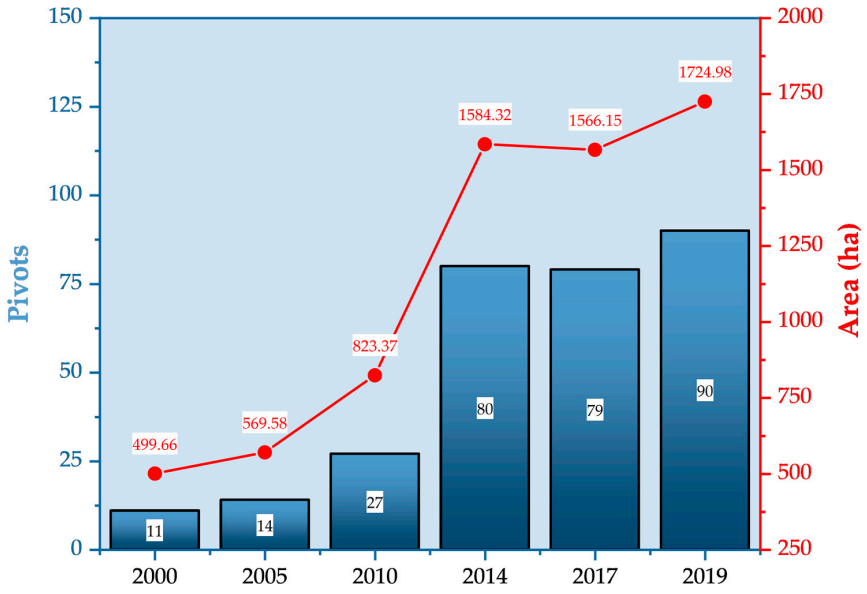

Figure 13. Estimation of area and number of center pivots in the study area in the period from 2000 to 2019.

5. Discussion

When compared to METRIC, SSEBop is considered a simpler alternative because it requires fewer input data and has more objective parameterization that facilitates its implementation without significant loss of precision in the ETa estimate [11,68]. Since 2015, ANA has been using the SSEBop-Br model to estimate water use in irrigated agriculture in Brazil, and the results have been very effective [11].

The irrigation balance is the difference between the ETa value and the precipitation that occurred during the crop cycle. It can be used as an indicator of irrigation water use considering that water supplementation is necessary when the precipitation is low. For the first cycle which occurs during the rainy season, the irrigation balance was negative for most classes. However, we cannot state that there was no irrigation because some crops have periods of high sensitivity to water deficit. For maize, this period is relatively short, and it goes from the flowering to the beginning of grain filling [69]. In addition, maize is one of the crops most affected by water deficits [70]. Although rainfall throughout the year is sufficient for summer crop cultivation, poor rain distribution can cause a drop in productivity. The occurrence of dry spells in the Cerrado region is very common, with dry periods in the middle of the rainy season [71]. In this situation, the producer can use center pivot irrigation to meet the crop's water demand during summer and then ensure that the productive potential is minimally affected.

The difference in the soy irrigation balance observed in the two cultivation types (single crop and first + second crop) can be explained by the planting date. Single-cycle soy is planted later, which extends to December in some cases. Soy in the first + second crop system (soy + potato) was grown until November. In single-cycle soy, the accumulated precipitation is lower (497.4 mm), which indicates that part of its cycle occurred in periods of lower precipitation and that water supplementation by irrigation was performed. In the first crop + winter crop, water use is concentrated in the second cycle due to the low precipitation level in the Cerrado region, which corroborates with the results obtained in our study.

The study area is characterized by the heterogeneous cultivation of vegetables, mainly potatoes and onions. In addition, there is an intense use of center pivot irrigation, which can reach up to three production cycles in one agricultural year [19,54]. This heterogeneity as well as the presence of more than one crop per pivot were identified through phenological metrics extracted from VI dense time series as proposed by Bendini et al. [19]. The use of phenological metrics allows us to infer the period in which the crop was in the field. Works related to irrigation water in agriculture at a large scale usually use fixed time intervals in the agriculture analysis.

The SSEBop-Br model estimates ETa from ETr, which in turn is obtained by the P-M method using three meteorological data sources. Wind speed, temperature, radiation, and relative air humidity are the main climatic variables used to estimate ETr [72,73]. Any variation in one of these variables can influence the result, and the radiation variable requires greater precision [74]. As INMET provides meteorological variables based on stations distributed across the country, it is expected that it best represents ETa in the Brazilian territory. However, no study confirms this fact. The variation of approximately 78% among the results obtained for the estimation of irrigation water use based on three meteorological data sources demonstrates the need to evaluate these data sources to guarantee more reliable results.

Crops of the first cycle presented negative irrigation balance, except for maize preceded by soy and soy crop cultivated in a single cycle, which presented values of up to 19.9 mm and 44.5 mm, respectively. A negative irrigation balance indicates that the precipitation supplied the crop water demand. However, if pivots were activated to supplement water demand caused by dry spells, it was not possible to quantify their use. All second-cycle crops showed positive irrigation balance, indicating water supplementation by pivots. This was expected, given that these crops were not planted in the rainy season.

The potato was the crop that used the most irrigation water, which was estimated at 2 million m^3 (INMET) and 1.3 million m^3 (CFSv2). Next, soy water use was estimated at 220,000 m^3 (CFSv2) and 800,000 m^3 (INMET). The irrigation water use for bean crops was estimated at 252,000 m^3 (CFSv2) and 333,000 m^3 (INMET). The water volume used for carrot irrigation was 52,000 m^3 (CFSv2) and 68,000 m^3 (INMET). Finally, irrigation water estimation for onion was 37,000 m^3 (CFSv2) and 98,000 m^3 (INMET). The total irrigation water volume used in the center pivots in the region of Itobi, SP, during the 2015/2016 agricultural year was 3.2 million m^3 (INMET), 2.5 million m^3 (GLDAS), and 1.8 million m^3 (CFSv2). The irrigation water use estimated for the same crop varied up to 72%, which depends on the meteorological data sources used for the ETa estimate.

6. Conclusions

This paper presents a method to estimate water use in irrigation agriculture combining phenological metrics and time series of ETa obtained by remote sensing technologies and precipitation data. Information regarding the phenological crop cycle, such as the beginning and the end of the cycle, was effective in the estimation of water use in irrigated crops. This allows us to infer the period when the crop is in the field. In addition, the use of phenological metrics extracted from the EVI time series was effective in classifying the crop within the mask of center pivots. The crops referring to the first cycle in the classes presented negative irrigation balance, except for the maize class preceded by soy, which presented water use of up to 19.9 mm, and the soy crop cultivated in a single cycle, which presented values of up to 44.5 mm. The negative irrigation balance indicates that the precipitation supplied the water demand for the crops. However, if the pivots were activated to supplement the water demand caused by dry spells, it was not possible to quantify the water use in these cases. The crops referring to the second cycle showed positive irrigation balance in all cases, indicating that there was water supplementation by the pivots, which was expected since these crops were not planted in the rainy season. Potato was the crop that used the most irrigation water, followed by soy, bean, carrot, and onion. The total irrigation water used by center pivots ranged from 3.2 million m^3 (INMET) to 1.8 million m^3 (CFSv2). In addition, the irrigation water use for the same crop varied up to 72%, depending on the meteorological data sources used for the ETa estimate. In future work, we suggest evaluating the meteorological data source's performance to generate more assertive irrigation water use estimates. In addition, we suggest scaling up the methodology proposed in this work to larger regions, such as for the entire Cerrado Biome. This work is in the context of the project "Irrigated Agriculture Based on Remote Sensing Technologies to Update and Improve ANA's Atlas Irrigation", developed by INPE and ANA (Process CNPq 423959/2021-2), which aims at developing a method for automatically mapping irrigated agricultural land and estimating water use in Brazilian irrigated agriculture.

Supplementary Materials: The following supporting information can be downloaded at: https://www.mdpi.com/article/10.3390/rs14235929/s1, Table S1: List of phenological metrics.

Author Contributions: Conceptualization, M.F.d.S.J., L.M.G.F. and H.d.N.B.; Methodology, M.F.d.S.J., L.M.G.F. and H.d.N.B., Supervision L.M.G.F. and H.d.N.B.; Writing—original draft, M.F.d.S.J.; Visualization, M.F.d.S.J.; Writing—review and editing, L.M.G.F., H.d.N.B. and M.F.d.S.J. All authors have read and agreed to the published version of the manuscript.

Funding: This research was funded by the National Council for Scientific and Technological Development (CNPq-Brazil) [Grant Number: 131046/2020-9], the Brazilian Space Agency (AEB) and Brazilian National Institute for Space Research (INPE).

Acknowledgments: This work used Landsat 7 and 8 (ETM+ and OLI sensors), courtesy of the U.S. Geological Survey. The authors acknowledge IAG-USP and the National Agency for Water and Basic Sanitation (ANA) for sharing the evapotranspiration field data. The authors also acknowledge Brazil Data Cube (a project part of the "Environmental Monitoring of Brazilian Biomes", funded by the Amazon Fund through the financial collaboration of the Brazilian Development Bank (BNDES) and the Foundation for Science, Technology and Space Applications (FUNCATE) no. 17.2.0536.1)

for the availability of the CBERS4A/AWFI mosaic. The authors are also grateful to the many individuals working on the development of free and open-source software for supporting the sharing of knowledge.

Conflicts of Interest: The authors declare no conflict of interest.

References

1. Agência Nacional de Águas. *Atlas Irrigação: Uso Da Água Na Agricultura Irrigada*, 2nd ed.; Agência Nacional de Águas: Brasilia, Brazil, 2021; p. 130.
2. Agência Nacional de Águas. *Polos Nacionais De Agricultura Irrigada*; Agência Nacional de Águas: Brasilia, Brazil, 2020; p. 26.
3. Dalin, C.; Taniguchi, M.; Green, T.R. Unsustainable Groundwater Use for Global Food Production and Related International Trade. *Glob. Sustain.* **2019**, *2*, e12. [CrossRef]
4. Davis, K.F.; Rulli, M.C.; Garrassino, F.; Chiarelli, D.; Seveso, A.; D'odorico, P. Water Limits to Closing Yield Gaps. *Adv. Water Resour.* **2017**, *99*, 67–75. [CrossRef]
5. Getirana, A.C.V.; Malta, V.F. Decision Process in a Water Use Conflict in Brazil. *Water Resour. Manag.* **2020**, *22*, 103–118. [CrossRef]
6. Xu, C.; Gong, L.; Jiang, T.; Chen, D.; Singh, V.P. Analysis of spatial distribution and temporal trend of reference evapotranspiration and pan evaporation in Changjiang (Yangtze River) catchment. *J. Hydrol.* **2006**, *327*, 81–93. [CrossRef]
7. Bhattarai, N.; Wagle, P. Recent Advances in Remote Sensing of Evapotranspiration. *Remote Sens.* **2021**, *13*, 4260. [CrossRef]
8. Wanniarachchi, S.; Sarukkalige, R. A Review on Evapotranspiration Estimation in Agricultural Water Management: Past, Present, and Future. *Hydrology* **2022**, *9*, 123. [CrossRef]
9. Schauer, M.; Senay, G.B. Characterizing crop water use dynamics in the Central Valley of California using Landsat-derived evapotranspiration. *Remote Sens.* **2019**, *11*, 1782. [CrossRef]
10. Mhawej, M.; Faour, G. Open-source Google Earth Engine 30-m evapotranspiration rates retrieval: The SEBALIGEE system. *Environ. Model. Softw.* **2020**, *133*, 104845. [CrossRef]
11. Agência Nacional de Águas. *Estimativa De Evapotranspiração Real Sensoriamento Remoto No Brasil*; Agência Nacional de Águas: Brasilia, Brasil, 2020; p. 41.
12. Casassola, A. Caracterização da Atividade Agrícola de Pivôs Centrais Por Meio de Séries Temporais de Imagens Sentinel-2 para Estimativas de Uso da Água na Agricultura Irrigada. Master's Thesis, Instituto Nacional de Pesquisas Espaciais, São José dos Campos, Brazil, 2022.
13. Rudorff, B.F.T.; Aguiar, D.A.; Silva, W.F.; Sugawara, L.M.; Adami, M.; Moreira, M.A. Studies on the rapid expansion of sugarcane for ethanol production in São Paulo State (Brazil) using landsat data. *Remote Sens.* **2010**, *2*, 1057–1076. [CrossRef]
14. Borges, E.F.; Sano, E.E. Séries temporais de EVI do MODIS para o mapeamento de uso e cobertura vegetal do oeste da Bahia. *Bol. Cienc. Geod.* **2014**, *20*, 526–547. [CrossRef]
15. Gusso, A.; Formaggio, A.R.; Rizzi, R.; Adami, M.; Rudorff, B.F.T. Soybean crop area estimation by Modis/Evi data. *Pesq. Agropec. Bras.* **2012**, *47*, 425–435. [CrossRef]
16. Arvor, D.; Jonathan, M.; Meirelles, M.S.O.P.; Dubreuil, V.; Durieux, L. Classification of MODIS EVI time series for crop mapping in the state of Mato Grosso, Brazil. *Int. J. Remote Sens.* **2011**, *32*, 7847–7871. [CrossRef]
17. Victoria, D.C.; Paz, A.R.; Coutinho, A.C.; Kastens, J.; Brown, J.C. Cropland area estimates using Modis NDVI time series in the state of Mato Grosso, Brazil. *Pesquisa Agropecuária Brasileira.* **2012**, *47*, 1270–1278. [CrossRef]
18. Bendini, H.N. Agricultural land classification based on phenological information from dense time-series Landsat-like images in the Brazilian Cerrado. Ph.D.'s Thesis, Instituto Nacional de Pesquisas Espaciais, São José dos Campos, Brazil, 2018.
19. Bendini, H.N.; Garcia Fonseca, L.M.; Schwieder, M.; Korting, T.S.; Sanches, I.A.; Leitão, P.J.; Hostert, P. Detailed agricultural land classification in the Brazilian cerrado based on phenological information from dense satellite image time series. *Int. J. Appl. Earth Obs. Geoinf.* **2019**, *82*, 101872.
20. Senay, G.B. Satellite psychrometric formulation of the Operational Simplified Surface Energy Balance (SSEBop) model for quantifying and mapping evapotranspiration. *Appl. Eng. Agric.* **2018**, *34*, 555–566. [CrossRef]
21. Walter, I.A.; Allen, R.G.; Elliott, R.; Jensen, M.E.; Itenfisu, D.; Mecham, B.; Howell, T.A.; Snyder, R.; Brown, P.; Echings, S.; et al. ASCE's standardized reference evapotranspiration equation. In Proceedings of the Watershed Management and Operations Management 2000, Fort Collins, CO, USA, 20–24 June 2000; pp. 1–11.
22. Senay, G.B.; Bohms, S.; Singh, R.K.; Gowda, P.H.; Velpuri, N.M.; Alemu, H.; Verdin, J.P. Operational Evapotranspiration Mapping Using Remote Sensing and Weather Datasets: A New Parameterization for the SSEB Approach. *J. Am. Water Resour. Assoc.* **2013**, *49*, 577–591. [CrossRef]
23. Setzer, J. *Atlas Climatológico E Ecológico Do Estado De São Paulo*; Comissão Interestadual da Bacia Paraná-Uruguai: São Paulo, Brazil, 1966; p. 61.
24. Cabral, O.M.R.; Rocha, H.R.; Gash, J.H.; Ligo, M.A.V.; Tatsch, J.D.; Freitas, H.C.; Brasilio, E. Water use in a sugarcane plantation. *GCB Bioenergy* **2012**, *4*, 555–565. [CrossRef]
25. Comitê Da Bacia Do Pardo. Deliberação CBH-PARDO 009/05, Governo do Estado de São Paulo, São Paulo, SP, Brasil. Ribeirão Preto. 2005. Available online: https://sigrh.sp.gov.br/public/uploads/deliberation//3632/009-declara-critica-a-bacia-do-ribeirao-das-congonhas.htm (accessed on 11 November 2021).

26. Liu, H.Q.; Huete, A. Feedback based modification of the NDVI to minimize canopy background and atmospheric noise. *IEEE Trans. Geosci. Remote. Sens.* **1995**, *33*, 457–465. [CrossRef]
27. Rufin, P.; Frantz, D.; Ernst, S.; Rabe, A.; Griffiths, P.; Özdoğan, M.; Hostert, P. Mapping cropping practices on a national scale using intra-annual Landsat time series binning. *Remote Sens.* **2019**, *11*, 232. [CrossRef]
28. Tatsch, J.D. Uma Análise dos Fluxos de Superfície e do Microclima Sobre Cerra, Cana-de-Açúcar e Eucalipto, com Implicações para Mudanças Climáticas Regionais. Master's Thesis, Universidade de São Paulo, São Paulo, Brazil, 2006.
29. Twine, T.E.; Kustas, W.P.; Norman, J.M.; Cook, D.R.; Houser, P.R.; Meyers, T.P.; Prueger, J.H.; Starks, P.J.; Wesely, M.L. Correcting eddycovariance flux underestimates over a grassland. *Agric. Meteorol.* **2000**, *103*, 279–300. [CrossRef]
30. De la Fuente-Sáiz, D.; Ortega-Farías, S.; Fonseca, D.; Ortega-Salazar, S.; Kilic, A.; Allen, R. Calibration of metric model to estimate energy balance over a drip-irrigated apple orchard. *Remote Sens.* **2017**, *9*, 670. [CrossRef]
31. Oliveira, B.S. Otimização do modelo Metric para estimativas de evapotranspiração no Cerrado brasileiro. Ph.D.'s Thesis, Instituto Nacional de Pesquisas Espaciais, São José dos Campos, Brazil, 2018.
32. Irmak, S.; Haman, D.Z. *Evapotranspiration: Potential or Reference?* Department of Agricultural and Biological Engineering- UF/IFAS Extension: Gainesville, FL, USA, 2017; p. 2.
33. Sanches, I.D.; Feitosa, R.Q.; Diaz, P.M.A.; Soares, M.D.; Luiz, A.J.B.; Schults, B.; Maurano, L.E.P. Campo Verde Database: Seeking to Improve Agricultural Remote Sensing of Tropical Areas. *IEEE Geosci. Remote Sens. Lett.* **2018**, *15*, 369–373. [CrossRef]
34. Soares, A.R.; Bendini, H.N.; Vaz, D.V.; Uehara, T.D.T.; Neves, A.K.; Lechler, S.; Korting, T.S.; Fonseca, L.M.G. STMETRICS: A Python Package for Satellite Image Time-Series Feature Extraction. In Proceedings of the IGARSS 2020: 2020 IEEE International Geoscience and Remote Sensing Symposium, Virtual Symposium, Virtual Symposium, 26 September 2020–2 October 2020.
35. Jönsson, P.; Eklundh, L. TIMESAT—A program for analyzing time-series of satellite sensor data. *Comput. Geosci.* **2004**, *30*, 833–845. [CrossRef]
36. Jönsson, P.; Eklundh, L. *TIMESAT 3.2 with Parallel Processing Software Manual*; Lund University: Lund, Sweden, 2015; pp. 22–24.
37. Harvey, A.C. *Forecasting, Structural Time Series Models and the Kalman Filter*; Cambridge University Press: Cambridge, UK, 1990.
38. Dougherty, R.L.; Edelman, A.S.; Hyman, J.M. Nonnegativity-, monotonicity-, or convexity-preserving cubic and quintic Hermite interpolation. *Math. Comput.* **1989**, *52*, 471–494. [CrossRef]
39. Breiman, L. Random Forests. *Mach. Learn.* **2001**, *45*, 5–32. [CrossRef]
40. Liaw, A.; Wiener, M. Classification and regression by randomforest. *R. News* **2002**, *2*, 18–22.
41. Belgiu, M.; Dragut, L. Random Forest in remote sensing: A review of applications and future directions. *ISPRS J. Photogramm. Remote Sens.* **2016**, *114*, 24–31. [CrossRef]
42. Rubinstein, R.; Kroese, D. *Simulation and the Monte Carlo Method*, 3rd ed.; Wiley—Interscience: Hoboken, NJ, USA, 2008; pp. 1–340.
43. Chinchor, N.; Sundheim, B. MUC-5 evaluation metrics. In Proceedings of the 5th Conference on Message Understanding, Stroudsburg, PA, USA, 25–27 August 1993.
44. Shapiro, D.E. The interpretation of diagnostic tests. Stat. *Methods Med. Res.* **1999**, *8*, 113–134. [CrossRef]
45. Xavier, A.C.; King, C.W.; Scanlon, B.R. Daily gridded meteorological variables in Brazil (1980–2013). *Int. J. Climatol.* **2016**, *36*, 2644–2659. [CrossRef]
46. Senay, G.B.; Friedrichs, M.; Singh, R.K.; Velpuri, N.M. Evaluating Landsat 8 evapotranspiration for water use mapping in the Colorado River Basin. *Remote Sens. Environ.* **2016**, *185*, 171–185. [CrossRef]
47. Willmott, C.J.; Matsuura, K. Advantages of the mean absolute error (MAE) over the root mean square error (RMSE) in assessing average model performance. *Clim. Res.* **2005**, *30*, 79–82. [CrossRef]
48. Sorooshian, S.; Duan, Q.; Gupta, V.K. Calibration of rainfall-runoff models: Application of global optimization to the Sacramento Soil Moisture Accounting Model. *Water Resour. Res.* **1993**, *29*, 1185–1194. [CrossRef]
49. Willmott, C.J. On the validation of models. *Phys. Geogr.* **1981**, *2*, 184–194. [CrossRef]
50. Nash, J.E.; Sutcliffe, J.V. River flow forecasting through conceptual models. Part 1: A discussion of principles. *J. Hydrol.* **1970**, *10*, 282–290. [CrossRef]
51. Van Liew, M.W.; Veith, T.L.; Bosch, D.D.; Arnold, J.G. Suitability of SWAT for the Conservation effects assessment project: A comparison on USDA-ARS watersheds. *J. Hydrol. Eng.* **2007**, *12*, 173–189. [CrossRef]
52. Agência Nacional de Águas; National Institute for Space Research. *Colaboração ANA-INPE Para O Atlas Irrigação 2021: Monitoramento De Pivôs Centrais Nos Polos De Agricultura Irrigada Do Cerrado*; Nota Técnica Conjunta, Nº 3/2021/SPR/INPE; Agência Nacional de Águas (ANA), Ed.; Agência Nacional de Águas (ANA): Brasília, Brazil, 2021.
53. Naghedifar, S.M.; Ziaei, A.N.; Ansari, H. Simulation of irrigation return flow from a Triticale farm under sprinkler and furrow irrigation systems using experimental data: A case study in arid region. *Agric. Water Manag.* **2018**, *210*, 185–197. [CrossRef]
54. Silveira, J.M.d.C.; Lima Júnior, S.d.; Sakai, E.; Matsura, E.E.; Pires, R.C.d.M.; Rocha, A.M. Identificação de áreas irrigadas por pivô central na sub-bacia tambaú-verde utilizando imagens ccd/cbers. *Irriga* **2013**, *18*, 721–729. [CrossRef]
55. Radin, B. Evapotranspiração máxima do milho medida em lisímetro e estimada pelo modelo de Penman-Monteith modificado. Master's Thesis, Federal University of Rio Grande do Sul, Porto Alegre, Brazil, 1998.
56. Alves, É.S. Evapotranspiração atual da cultura de soja: Modelagem e avaliação da evaporação direta da água do solo. Ph.D. Thesis, Universidade Federal de Viçosa, Viçosa, Brazil, 2020.
57. Allen, R.G.; Pereira, L.S.; Raes, D.; Smith, M. *Crop Evapotranspiration—Guidelines for Computing Crop Water Requirements*; FAO Irrigation and Drainge: Rome, Italy, 1998; p. 56.

58. EMBRAPA. *Tecnologias De Produção De Soja: Região Central Do Brasil, 2001*; Embrapa Soja: Londrina, Brazil, 2002; p. 199.
59. EMBRAPA. *Tecnologias De Produção De Soja—Região Central Do Brasil*; Embrapa Cerrados: Planaltina, Brazil, 2011; p. 21.
60. Lunardi, D.M.C.; Filho, J.L. Evapotranspiração máxima e coeficiente de cultura da cenoura (*Daucus carota* L.). *Rev. Bras. Agrometeorol.* **1999**, *7*, 13–17.
61. Moura, M.V.T.; Marques Júnior, S.; Brotel, T.A.; Frizone, J.A. Estimativa do consumo de água da cultura da cenoura (*Daucus carota*, L.) v. Nantes Superior, para a região de Piracicaba, através do Balanço Hídrico. *Sci. Agric.* **1994**, *51*, 284–291. [CrossRef]
62. EMBRAPA. *Irrigação Da Cultura Da Cenoura (Circular Técnica, 48)*; Embrapa Hortaliças: Brasília, Brazil, 2007; p. 14.
63. Matzenauer, R.; Maluf, J.R.T.; Bueno, A.C. Evapotranspiração da cultura do feijão e sua relação com a evaporação do tanque classe "A". *Pesqui. Agropecuária Gaúcha* **1998**, *4*, 101–106.
64. EMBRAPA. *Conhecendo A Fenologia Do Feijoeiro E Seus Aspectos Fitotécnicos*; Embrapa Arroz e Feijão: Brasilia, Brazil, 2018; p. 59.
65. EMBRAPA. *Irrigação Na Cultura Da Cebola, (Circular Técnica, 37)*; Embrapa Hortaliças: Brasília, Brazil, 2005; p. 17.
66. Associação Brasileira da Batata. *Irrigação Na Cultura Da Batata*; Associação Brasileira da Batata: Itapetininga, Brazil, 2006; p. 66.
67. Agência Nacional de Águas. *Levantamento Da Agricultura Irrigada Por Pivôs Centrais No Brasil*; Agência Nacional de Águas: Brasília, Brazil, 2019; p. 49.
68. Mcshane, R.R.; Driscoll, K.P.; Sando, R. *A Review of Surface Energy Balance Models for Estimating Actual Evapotranspiration with Remote Sensing at High Spatiotemporal Resolution over Large Extents*; U.S. Geological Survey Scientific Investigations Report 2017–5087; US Geological Survey: Reston, VA, USA, 2017; p. 19.
69. Matzenauer, R.; Bergamaschi, H.; Berlato, M.A.; Maluf, J.R.T.M.; Barni, N.A.; Bueno, A.C.; Didone, I.A.; Anjos, C.S.d.; Machado, F.A.; Sampaio, M.d.R. *Consumo De Água E Disponibilidade Hídrica Para Milho E Soja No Rio Grande Do Sul*; Fepagro: Porto Alegre, Brazil, 2002; p. 105.
70. Radin, B.; Bergamaschi, H.; Santos, A.O.; Bergonci, J.I.; França, S. Evapotranspiração da cultura do milho em função da demanda evaporativa atmosférica e do crescimento das plantas. *Pesq. Agrop.* **2003**, *9*, 7–16.
71. EMBRAPA. *Viabilidade E Manejo Da Irrigação Da Cultura Do Milho (Embrapa Milho. Circular Técnica, 85)*; Embrapa Milho: Sete Lagoas, Brazil, 2006; p. 12.
72. Darshana; Pandey, A.; Pandey, R.P. Analysing trends in reference evapotranspiration and weather variables in the Tons River Basin in Central India. *Stoch. Environ. Res. Risk Assess.* **2013**, *27*, 1407–1421. [CrossRef]
73. Matzenauer, R. Evapotranspiração de plantas cultivadas e coeficientes de cultura. In *BERGAMASCHI, H. (Coord.). Agrometeorologia aplicada à irrigação*; Editora da UFRGS: Porto Alegre, Brazil, 1992; pp. 33–49.
74. Lemos Filho, L.C.A.; Carvalho, L.G.; Evangelista, A.W.P.; Júnior, J.A. Análise espacial da influência dos elementos meteorológicos sobre a evapotranspiração de referência em Minas Gerais. *Rev. Bras. De Eng. Agrícola E Ambient.* **2010**, *14*, 1294–1303. [CrossRef]